Intercomparison of Gravity Wave Parameterizations: Hines Doppler-Spread and Warner and McIntyre Ultra-Simple Schemes

Martin CHARRON, Elisa MANZINI

Max-Planck-Institut für Meteorologie, Hamburg, Germany

and

Christopher D. WARNER

Centre for Atmospheric Science, Department of Applied Mathematics and Theoretical Physics, University of Cambridge, Cambridge, United Kingdom

(Manuscript received 23 May 2001, in revised form 29 October 2001)

Abstract

The "three-part ultra-simple" gravity wave parameterization of Warner and McIntyre is compared with the "Doppler-spread" parameterization of Hines. The two parameterizations are tested on a background state at rest with constant buoyancy frequency, as well as on background states defined by the CIRA86 data at 70N in July and January. To achieve as clean a comparison as possible between the two parameterizations, two approaches are taken. The first approach is to adjust the free parameters to obtain the same source level momentum fluxes, and as similar a source spectrum shape, as is possible. The second approach is to adjust the source level momentum fluxes to obtain the same momentum fluxes at mesospheric altitudes. The resulting vertical profiles of the momentum fluxes, of the wave-induced forces, and of the energy dissipation rates produced by the two parameterizations are compared.

When a similar gravity wave source spectrum is used, specifically the source spectrum recommended by Hines, momentum deposition generally tends to occur lower in the atmosphere for the Warner and McIntyre parameterization than for the Hines Doppler-spread parameterization. In order to obtain similar wave-induced forces, and dissipation rates in the mesosphere from the two parameterizations, it has been found that the Warner and McIntyre parameterization requires the source spectrum to be scaled so that the net momentum flux in the lower stratosphere is an order of magnitude higher than the Hines Doppler-spread parameterization.

1. Introduction

Small scale gravity waves arising from non-stationary and non-orographic tropospheric sources are thought to play a crucial role in the momentum budget of the circulation of the middle and upper atmosphere (see for example Hamilton (1997) and references therein). In the context of a numerical simulation of the global middle and upper atmospheric circulation at a relatively low resolution, these waves must be parameterized in order to get a model climatology that is comparable to observations. A number of parameterizations (Medvedev and Klassen 1995; Hines 1997a,b; Warner and McIntyre 1999, 2001) have aimed to represent the effects on the middle and upper atmosphere of a broad spectrum of unresolved gravity waves emerging from a variety of sources. They have been de-

Corresponding author: Elisa Manzini, Max-Planck-Institut fur Meteorologie, Bundesstrasse 55, 20146 Hamburg, Germany.
E-mail: manzini@dkrz.de

veloped and tested in various general circulation models (GCMs) (Medvedev et al. 1998; Manzini and McFarlane 1998; Scaife et al. 2000).

These parameterizations require sensible, but often poorly constrained, choices of adjustable (free) parameters to be made—choices to which model simulations are very sensitive. This situation brings about the possibility that different gravity wave parameterizations, based on inherently different basic principles on how gravity waves are propagated and dissipated, can give rise to similar results in a given GCM just because these free parameters have been adjusted with the aim of obtaining a reasonably realistic climatology of the middle atmosphere circulation.

The purpose of this paper is to compare two gravity wave parameterizations by means of "off line" calculations (e.g., diagnosing the gravity wave-induced force and energy dissipation, for given background states). The motivation is to better understand their relative behavior, and advantages or disadvantages that can be encountered, when the parameterizations are used in GCMs. The parameterizations considered here are the Doppler-spread parameterization of Hines (1997a,b) (hereafter HDS), and the three part ultra-simple spectral parameterization of Warner and McIntyre (2001) (hereafter WM). To achieve as clean a comparison as possible between the two parameterizations, two approaches are taken. The first approach is to adjust the free parameters to obtain the same source level momentum fluxes and as similar a source spectrum shape as is possible. The source spectrum chosen is that recommended in Hines (1997a,b). The second approach is to adjust the source level momentum fluxes by scaling the launch spectrum for the WM parameterization, to obtain the same momentum fluxes at mesospheric altitudes.

2. Brief description of the two parameterizations

The major difference between the two considered parameterizations is in the way they represent gravity wave dissipation. In the framework of the HDS model (Hines 1991a,b,c, and Hines 1993), the wave spectral elements most likely to dissipate are the ones with relatively short vertical wavelengths and slow phase speeds, meaning that nonlinear advection might well be fundamental in the initiation of the dissipation process. This nonlinear advection is thought to give rise to Doppler spreading. The WM parameterization, on the other hand, imposes gravity wave saturation by employing an empirical criterion, derived from gravity wave observational studies (see, for example, Tsuda et al. 1991; Smith et al. 1987), that limits the growth of the vertical wavenumber spectrum of the gravity wave field.

However, the parameterizations use similar simplifications to the gravity wave propagation problem in order to achieve computational efficiency. The common simplifications include neglecting Coriolis and non-hydrostatic effects, and back-reflection, under which conditions it turns out that the gravity wave spectrum can be expressed as a function of vertical wavenumber only. Thus, in WM the frequency dependence is integrated out, while in HDS the horizontal wavenumber dependence is integrated out. In both cases, the problem is reduced to modelling the evolution of the vertical wavenumber energy spectrum. For a complete description, the reader is referred to Hines (1997a,b) and Warner and McIntyre (2001).

In the WM parameterization, very simple idealized spectral shapes are used to allow for the analytical integration of vertical wavenumber pseudomomentum flux spectrum. The vertical wavenumber dependence of the spectrum is modelled by assuming that it consists of, at most, three analytically integrable segments. These segments can be of three types: conservatively propagated from the launch altitude; saturated at the current altitude; or, saturated at a lower altitude then conservatively propagated to the current altitude. These three types of segment can represent well a wide range of possible spectral shapes. Gravity waves are assumed to propagate vertically, without interacting with each other, while being Doppler-shifted by the background winds. Dissipation, or wave-breaking, is represented by imposing a limiting saturation spectrum proportional to m^{-3}, where m is the vertical wavenumber. As already stated, the m^{-3} shape has been found in many observational studies.

The essence of the WM parameterization is to propagate the idealized spectrum conservatively through an altitude increment, then to

impose as a limit the saturation spectrum to those parts of the conservatively propagated spectrum that are greater than the saturation spectrum, then, if required, to define a new idealized spectrum shape. This calculation is carried out in turn for four azimuthal directions of propagation. The total momentum flux (area under the spectrum) for each propagation direction, and altitude level, is used to calculate the total energy flux, the wave-induced force, and the energy dissipation rate.

In the HDS framework (Hines 1991a,b,c, and Hines 1993), nonlinear advection by the gravity wave field is intended to be taken into account by Doppler spreading, in a statistical sense, the vertical wavenumber spectrum towards high vertical wavenumbers. In this parameterization, gravity wave breaking is represented by imposing an upper limit to the range of vertical wavenumbers in the spectrum that can propagate above the altitude considered. If in a particular azimuth j and at an altitude z, the wavenumber upper limit is denoted $m_j(z)$, any spectral element in the j azimuth with a vertical wavenumber greater than m_j is considered to be dissipated and is removed, thus producing momentum flux deposition at altitude z. Moreover, $m_j(z)$ is prescribed to be constant or to decrease with altitude, forbidding spontaneous gravity wave generation above the source level.

The calculation of $m_j(z)$ includes the effects of Doppler spreading from the gravity waves, Doppler shifting by the background winds, and instability of the gravity wave system. It is given by

$$m_j = \frac{N_0}{\Phi_1 \hat{\sigma}_j + \Phi_2 \hat{\sigma}_h + V_j - V_{0j}},$$

where N_0 is the buoyancy frequency at the initial level, $\hat{\sigma}_j$ is the gravity wave j-wind standard deviation at altitude z, $\hat{\sigma}_h$ is the total gravity wave wind standard deviation at altitude z, V_j is the background wind in direction j at altitude z, V_{0j} is the background wind in direction j at initial altitude, Φ_1 and Φ_2 are adjustable parameters with ranges that are estimated theoretically in Hines (1993, 1997a). The energy dissipation rate modelled by the HDS parameterization is proportional to another adjustable parameter Φ_5, that is also constrained by the theory. Other adjustable parameters, which are dependent on the gravity wave generation mechanisms that are to be parameterized, are also needed in the HDS framework. These include an equivalent horizontal wavenumber $k^\star$, which represents the mean horizontal wavelength of the gravity wave spectrum, a lower bound vertical wavenumber $m_{\min}$, which limits the allowable maximum vertical wavelength of the spectrum, and the standard deviation in azimuth j of the horizontal gravity wave wind at the generation level.

3. Intercomparison

The purpose is to compare the two parameterizations for a vertical wavenumber spectrum at the source level as similar as possible, both in shape and in total momentum flux. Similar source spectra are achieved for both parameterizations by specifying a vertical wavenumber lower bound of $2\pi/(20\text{ km})$, to avoid unrealistically large vertical wavelengths, and a small-m slope of 1 (unless otherwise specified). The HDS vertical wavenumber energy spectrum has an upper bound vertical wavenumbers value of m_j at the source level (this value is explicitly determined by the HDS scheme). In the case of the WM, the source level value for the crossover vertical wavenumber (which is the peak of the WM spectrum) m_{x_1}, is set to $2\pi/(0.5\text{ km})$, a value close to m_j at the source level. For wavenumbers larger than m_{x_1}, a steep source spectrum shape m^{-15} is employed, making the HDS and WM source spectra very similar. A consequence of this choice is that the source level WM spectrum is not saturated, since the saturation function has shape m^{-3}.

All experiments employ an initial azimuthally isotropic spectrum located at an altitude of 4.2 km. Table 1 summarizes the free parameters that have been employed (the notation is similar to Hines (1997a,b) and Warner and McIntyre (2001)). In the three cases described below, the HDS equivalent horizontal wavelength is 125 km. The source level total wind variance is 0.5 $\text{m}^2\ \text{s}^{-2}$ (unless otherwise specified). In the WM case, the momentum flux in an azimuthal sector is proportional to an adjustable parameter β. The cases $\beta \sim 0.1$, and $\beta \sim 1$ have been studied.

Three off-line experiments have been performed: The first one uses a background state at rest with constant buoyancy frequency, the

Table 1. Parameter setting for the Warner and McIntyre (WM) and Hines (HDS) schemes.

Scheme	Parameter	Description
WM	$s = 1$ and 2	slope of the first part of the vertical wavenumber spectrum
	$t = 3$	(-) slope of the chopping vertical wavenumber spectrum
	$p = 5/3$	(-) slope of the frequency spectrum
	$\beta \sim 0.1$ and 1	empirical constant used in defining the momentum flux
	$m_{\mathrm{cut}} = 2\pi/(20\ \mathrm{km})$ and 0	minimum value of the vertical wavenumber
	$m_{\mathrm{x_1}} = 2\pi/(0.5\ \mathrm{km})$	cross over vertical wave number of the source spectrum
	$J = 4$	number of equally spaced azimuths
HDS	$s = 1$ and 2	slope of the vertical wavenumber source spectrum
	$m_{\mathrm{min}} = 2\pi/(20\ \mathrm{km})$ and 0	minimum value of the vertical wavenumber
	$J = 4$	number of equally spaced azimuths
	$\hat{\sigma}^2_{h0} = 0.5$ and 144 $\mathrm{m^2\ s^{-2}}$	source level total wind variance
	$k^\star = \frac{2\pi}{125\ \mathrm{km}}$ and $\frac{2\pi}{20000\ \mathrm{km}}$	equivalent horizontal wavenumber
	$\Phi_1 = 1.5$	azimuthal rms coefficient
	$\Phi_2 = 0.3$	total rms coefficient
	$\Phi_3 = 1.0$	coefficient used in calculation of maximum permissible molecular viscosity-induced cutoff wavenumber
	$\Phi_5 = 2.0$	coefficient used in calculation of dissipation rate

second one employs the CIRA86 atmosphere (Fleming et al. 1990) at 70N in July as the background state; and, the third uses the CIRA86 atmosphere at 70N in January.

3.1 *Background state at rest with constant buoyancy frequency*

This test evaluates the behavior of the parameterizations without taking into account the influence of the background state variations other than the decrease of density with height. It employs a uniform buoyancy frequency of 0.02 $\mathrm{s^{-1}}$, and no background wind.

For both parameterizations, the vertical flux of horizontal momentum in one given direction is shown as a function of altitude in Fig. 1, for three different spectra.

The upper left panel employs a spectral slope of value 1 for the small-m part of the spectra, and a lower bound vertical wavenumber of $2\pi/20$ km. The lower left panel employs a spectral slope of value 2 for the small-m part of the spectra, and a lower bound vertical wavenumber of 0 km. The settings employed for the upper right panel are identical to those of the upper left panel, except that β in WM is increased by a factor of about 10, and the source level wind variance in HDS is specified to be 2.9 $\mathrm{m^2\ s^{-2}}$. This sets an initial momentum flux in one direction that is ten times greater than what is employed to produce the upper left panel (note that m_{x_1} in WM is kept to $2\pi/(0.5$ km) while m_j at source level in HDS takes a slightly smaller value of $2\pi/(0.7$ km)). The solid curves refer

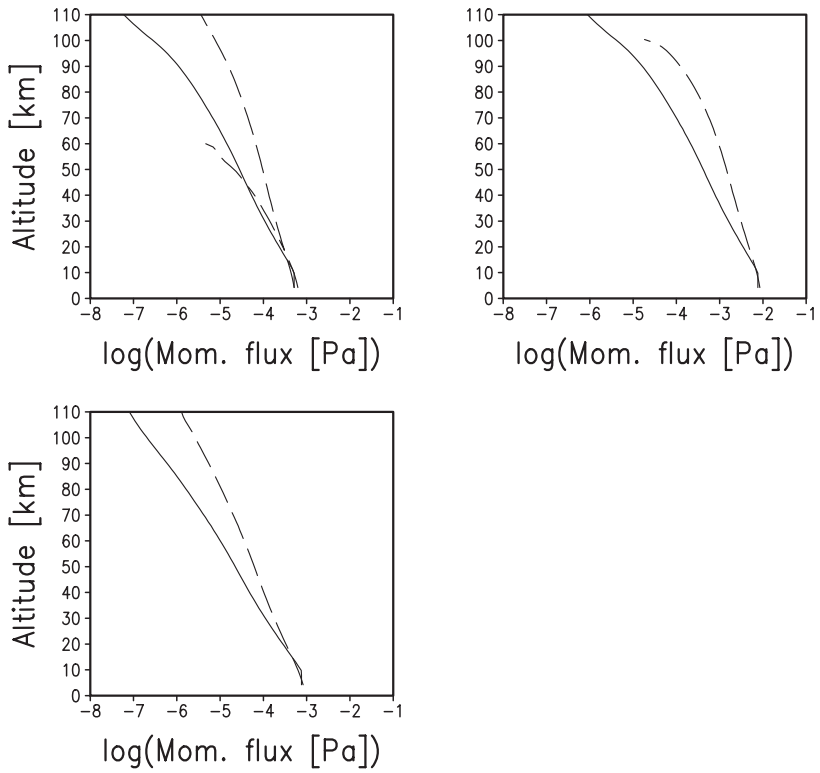

Fig. 1. Vertical profile of the $\log_{10}$ of the vertical flux of horizontal momentum in one direction for a background basic state at rest, with constant buoyancy frequency. Solid curve: WM parameterization; long dashed curve: HDS parameterization with $k^\star = 2\pi/(125$ km); long-short dashed curve: HDS parameterization with $k^\star = 2\pi/(20000$ km). Upper left panel: lower bound vertical wavenumber is $2\pi/(20$ km), spectral slope has value one. Upper right panel: as for upper left, but initial level momentum flux ten times greater. Lower left panel: lower bound vertical wavenumber is zero, spectral slope has value two.

to WM, the long dashed curves to HDS with $k^\star = 2\pi/125$ km, and the long-short dashed curve to HDS with $k^\star = 2\pi/20000$ km and wind variance of 144 m^2 s^{-2} (to keep the same momentum flux at the source level).

Above the source level, the momentum flux computed from the WM parameterization (solid curves) decreases at a faster rate with increasing height than that computed from the HDS parameterization (long dashed curve only) for the three spectra employed here. Therefore, in the WM parameterization less momentum flux remains at higher levels. In terms of momentum deposition (not directly seen from Fig. 1 since the logarithm of the momentum flux is shown), this means that the WM parameterization will produce stronger momentum deposition at lower levels than the HDS parameterization. Because the wave-induced acceleration is inversely proportional to density, momentum deposition at relatively low levels will generate small wave-induced forces, as is shown in the next section, for the case of realistic background atmospheric states. Note that to get a similar rate of momentum deposition as in the WM parameterization at low levels, an unrealistically large equivalent horizontal wavelength of several thousands kilometers must be specified in the HDS scheme (long-short dashed curve of the upper left panel). Adjustments to the other free parameters (Φ_1, Φ_2, and Φ_3), within the range proposed in Hines (1997a,b), or doubling the number of horizontal azimuths, does not modify substantially the behavior of the HDS parameterization in the present case (see McLandress, 1997).

Figure 1 shows that the HDS momentum flux profile is somewhat sensitive to a change of the

source level momentum flux in one direction (upper left versus upper right) and/or the spectral shape (upper left versus bottom), but the relative difference between the two parameterizations is retained.

It should be noted that for a specific spectral shape, the choice of m_{x_1} at source level in the WM scheme does not influence the behavior of the scheme as long as the source level momentum flux in one given direction is kept the same (i.e., changing β as well as m_{x_1} to keep the same amount of source level momentum flux will result in the same momentum flux vertical profile). This is because the momentum flux at altitude z is equal to the momentum flux at source level multiplied by a function that depends on density and spectral slopes only. Hence, the relative difference in WM and HDS is not due to the particular choice of m_{x_1} when the background wind is at rest. This explains why, in the upper left and right panels of Fig. 1, the WM curves are the same, but for a scaling factor.

The reason for such different behavior is intrinsic to how the vertical evolution of the momentum flux is represented in the two parameterizations. The HDS parameterization does not impose a saturation limit on the propagating part of the vertical wavenumber spectrum, while it totally obliterates waves that have become unstable (i.e., it removes the momentum transported by the obliterated waves at high vertical wavenumbers only). Thus the HDS parameterization can, and does, have spectral shapes that are well above the WM saturation limit, consistent with the assumption in the HDS that the m^{-3} shape is due to spreading of still propagating waves and not directly to instability. The WM parameterization instead imposes a saturation function, based on empirical evidence, that leads to a substantial portion of the total vertical wavenumber pseudo-momentum flux spectrum being dissipated in the lower stratosphere. This substantial dissipation is not primarily because of the simplifications used. Indeed, as shown by Warner and McIntyre (2001), in the case with no background wind variations, the WM parameterization represents fairly well the behavior of a more complete approach for the evolution of a full (frequency and wavenumber dependent) linear gravity wave spectrum, empirically saturated by a m^{-3} function.

On the other hand, the WM parameterization can have spectral shapes with waves above the HDS high vertical wavenumber obliteration limit.

Note that if the shape of the chopping spectral density of the WM scheme is changed to m^{-4}, the HDS and WM schemes behave in a very similar fashion (not shown). This is due to the fact that a steeper chopping function will affect less the part of the spectrum with vertical wavenumbers lower than m_{x_1} as defined at the source, though there is no empirical evidence for an m^{-4} shape.

3.2 *Background states provided by CIRA86 data*

Figure 2 shows the comparison between the two parameterizations for the momentum flux in eastward-propagating and westward-propagating azimuthal sectors, and the net zonal momentum flux (three left panels) as well as for the wave-induced force per unit mass and the dissipation rate (top two right panels). The CIRA86 zonal wind profile at 70N in July is shown in the bottom right panel. Note that the solid (WM) and long dashed (HDS) curves have the same amount of momentum flux, namely 7.8×10^{-4} Pa, at the source level, while the dotted curve is the WM parameterization with a larger initial momentum flux of 73.1×10^{-4} Pa ($\beta \sim 1$ instead of 0.1).

For both parameterizations, the eastward-propagating momentum flux (top left panel) that reaches the lower stratosphere is attenuated by the tropospheric eastward winds, just above the source level. Thereafter, the shear is negative for the considered azimuth, therefore initially there is no or weak momentum deposition. As might be expected from the previous case, for the WM parameterization the momentum deposition starts lower down, already in the stratosphere, while deposition occurs in the HDS only in the upper mesosphere. In order to get a similar eastward-propagating momentum flux profile for both parameterizations above 80 km, one has to use a WM momentum flux in each given azimuthal sector at the source about 10 times larger than the HDS value (compare the dotted line with the long dashed line in Fig. 2, upper left).

Alternatively, one could have reduced the momentum flux in HDS at the source level.

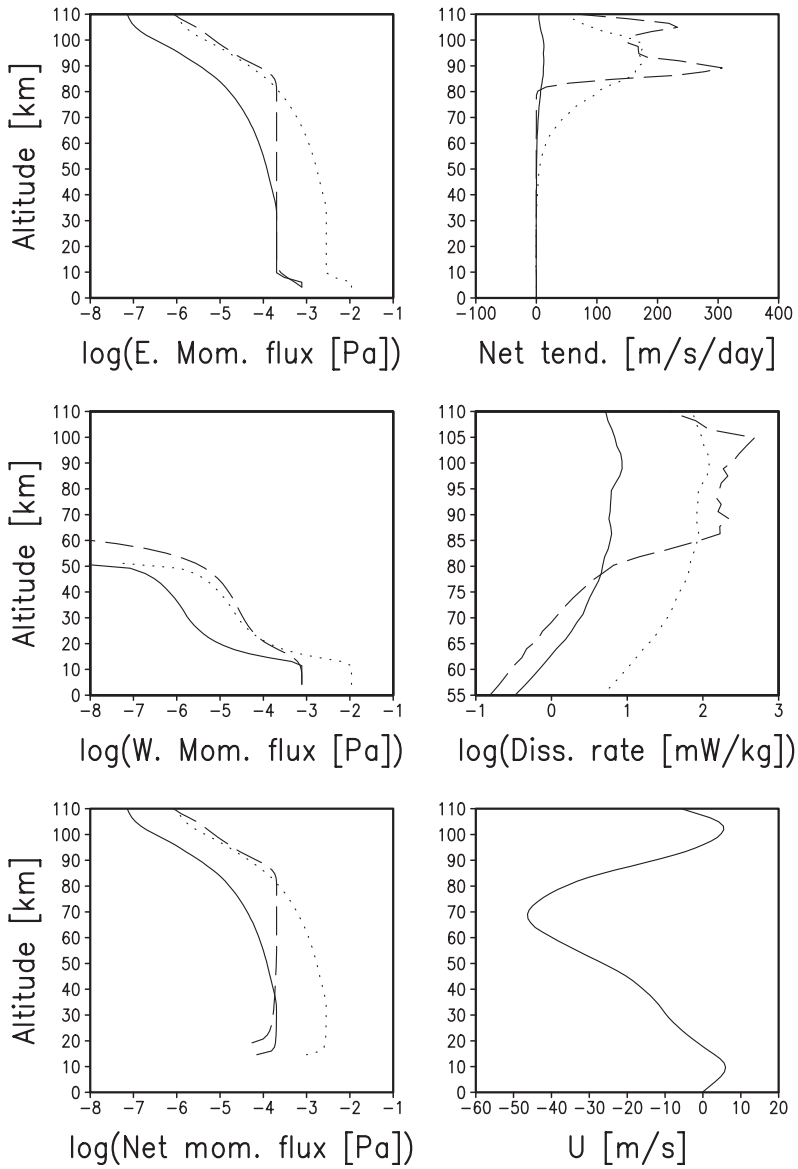

Fig. 2. Vertical profile of the $\log_{10}$ of vertical flux of horizontal momentum in the East direction (upper left panel), West direction (middle left panel), and of the net zonal flux (lower left panel, only positive values are shown) for the basic state given by the CIRA86 data at 70N in July. The solid curve and the dotted curve are from the WM parameterization, the long dashed curve is from the HDS parameterization. The momentum flux at the source level is 7.8×10^{-4} Pa in each cardinal direction for the solid and long dashed curves, while it is 7.3×10^{-3} Pa in each cardinal direction at the source level for the dotted curve. Upper right panel: vertical profile of the net induced force per unit mass (m s^{-1} day^{-1}). Middle right panel: vertical profile of the $\log_{10}$ of total energy dissipation rates per unit mass (mW kg^{-1}). The background zonal wind (m s^{-1}) is shown in the lower right panel.

In the case of the westward-propagating momentum flux (middle left panel), the momentum flux is completely deposited below 60 km (HDS) or 50 km (for both cases with WM). The net zonal momentum flux for the three cases considered is shown in the bottom left panel of Fig. 2 (only positive values are shown). The vertical evolution of the net zonal momentum

flux summarizes the results from the previous two panels. Also clear is the fact that for the cases with a comparable net momentum deposition in the upper mesosphere, that is the WM (dotted curve) and HDS (long-dashed curve), the net momentum flux that emerges from the troposphere is an order of magnitude greater for the WM case, than for the HDS case. In terms of the induced force per unit mass, (or the divergence of the net momentum flux), close to the mesopause, a difference of about an order of magnitude is found when the same momentum flux in an azimuthal sector (at the source level) is used. As expected from the net zonal momentum flux profile, the WM parameterization with larger momentum flux at the source level (dotted curve) does produce an induced force per unit mass comparable to that of the HDS parameterization. However, given that some of the WM momentum flux is deposited lower in the atmosphere, the WM parameterization produces a significant net induced force lower in the mesosphere than does the HDS, down to about 60 km. The WM profile of the induced force per unit mass, is therefore much smoother.

Another measure of the difference in the behavior of the two parameterizations is given by the total energy dissipation rates per unit mass (Fig. 2, middle right panel). Again, for similar source momentum fluxes, the HDS dissipation rates are about an order of magnitude larger. The HDS, and WM dissipation rates, are comparable only when the WM parameterization is initialized with larger momentum flux at the source level (long-dashed and dotted curves, respectively).

Values of energy dissipation rates in the mesosphere and lower thermosphere at high latitudes were derived by Lübken (1997) from rocket soundings that measure neutral density fluctuations down to a scale of a few meters. The shape and intensity of these profiles can be advantageously used to evaluate and compare gravity wave parameterizations, in the case that the turbulence these rocket soundings measure is mainly due to gravity wave breaking (or otherwise dissipating). Around 80–90 km, the HDS and the WM dissipation rates (second case, with larger source momentum flux) agree fairly well with Lübken (1997). However, the profiles of Lübken (1997) do not indicate any sign of turbulence below the 80 km altitude level at 70N in summer; the high values of dissipation rates appear abruptly near 80 km of altitude in the data. This is not seen with the WM scheme, which produces a relatively smooth increase of dissipation rates with altitude. However, the HDS does capture the rapid increase in dissipation rates with height.

Figure 3 shows a similar comparison of the three cases in Fig. 2, but this time for the CIRA86 basic state at 70N in January. Similar conclusions can be drawn for the vertical profiles of momentum fluxes, induced force and dissipation rates as for the July case. However, it is interesting to note that the energy dissipation rates derived from Lübken (1997), for the winter case, showed a much larger variability in the dissipation rate profiles, with values ranging two order of magnitudes, and a much deeper layer of the atmosphere affected by turbulence, from 60 to 100 km. For the winter case all the three profiles in Fig. 3 (middle right) are within the range of the Lübken (1997) estimates. Also, some of the measurements occurred in other winter months than January, therefore January CIRA86 background winds may not be the best choice.

4. Conclusions

The WM and HDS parameterizations have been tested in a controlled context with parameter settings that are as close to being equivalent as is possible, given the different basis of the two parameterizations. For such conditions, it has been found that the WM parameterization deposits momentum lower in the atmosphere than the HDS parameterization, allowing less momentum to reach the mesosphere and producing less induced force by, at least, an order of magnitude. The vertical profiles of wave-induced force and energy dissipation from the WM parameterization are generally smoother than those of the HDS parameterization. The former therefore extend deeper in the atmosphere, especially when the July CIRA86 basic state is used.

Both parameterizations can be adjusted to produce similar values of energy dissipation rates near the CIRA86 mesopause, that are comparable to those suggested by measurements at high latitude in summer. However, to obtain such dissipation rates, the net momen-

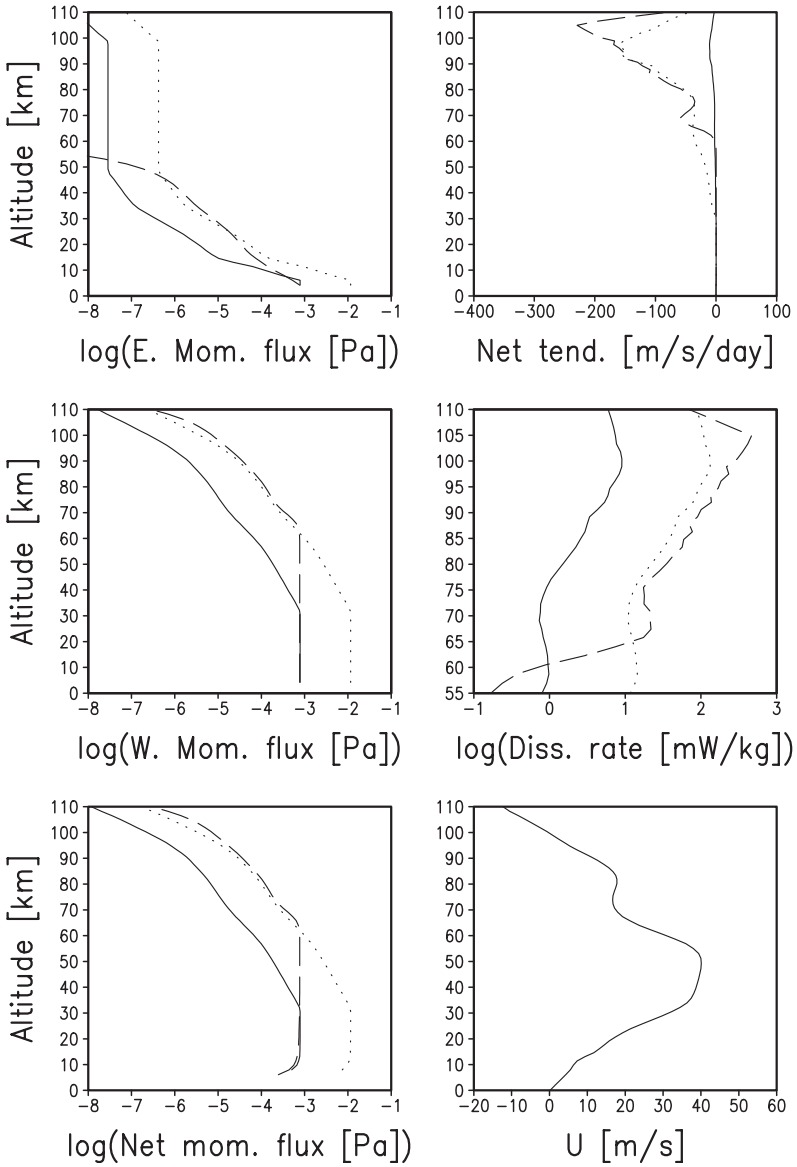

Fig. 3. As in Fig. 2, but for January.

tum flux that emerges from the troposphere is an order of magnitude larger for the WM parameterization than for the HDS parameterization.

The abrupt increase of dissipation rates starting at around 80 km of altitude measured in summer by Lübken (1997) is more realistically simulated with the HDS parameterization on the CIRA86 data, than with the WM parameterization. The WM parameterization produces smoother dissipation rates that start to be significant near the 60 km level.

It should be emphasized that to get a comparable launch spectrum, we chose here to adjust the launch spectrum of the WM parameterization to agree with that of the Hines parameterization. In particular, the launch spectrum employed with the background given by CIRA86, peaked at a vertical wavenumber of $2\pi/(0.5\text{ km})$, which is four times larger than the

value used in Warner and McIntyre (2001). However, in the case of the background state at rest, the choice of the location of the peak (in vertical wavenumber space), is of no importance since the evolution of the WM spectrum does not depend on it for a given source level momentum flux.

In principle, it would have been possible to adjust the launch spectrum of the HDS parameterization to fit the launch spectral parameters in Warner and McIntyre (2001)—a launch spectrum that is very different, especially for the important small-m waves that reach the mesosphere, than those launch spectra used in the present paper.

This work is an example showing that if systematic observations such as dissipation rates in the mesosphere (assessing the response of a parameterization) as well as momentum fluxes in the lower stratosphere (assessing the source forcing of a parameterization), were available, it could be possible to better evaluate and constrain currently available parameterizations.

It would be especially useful, though very difficult to achieve in practice, to be able to constrain with observations the small-vertical wavenumber shape of the gravity wave spectra, which contains those waves which are most likely to dissipate in the mesosphere.

Acknowledgments

The authors are thankful to Andreas Rhodin and Erich Roeckner for their comments on this manuscript. MC and EM acknowledge support from the Bundesministerium für Bildung und Forschung, Contract 07ATF 10 of the Atmosphärenforschung 2000 Programme, CDW received support from the Natural Environment Research Council through Grant GR3/1163, through the UK Universities' Global Atmospheric Modelling Project.

References

Fleming, E.L., S. Chandra, J.J. Barnett, and M. Corney, 1990: Zonal mean temperature, pressure, zonal wind and geopotential height as functions of latitude, *Adv. Space Rev.*, **10**, 1211–1259.

Fritts, D.C. and W. Lu, 1993: Spectral estimates of gravity wave energy and momentum fluxes, II, Parameterization of wave forcing and variability, *J. Atmos. Sci.*, **50**, 3695–3713.

Hamilton, K. (Ed.), 1997: *Gravity Wave Processes: Their Parameterization in Global Climate Models*, 401 pp., Springer-Verlag, Heidelberg.

Hines, C.O., 1991a: The saturation of gravity waves in the middle atmosphere. Part I: Critique of linear instability theory, *J. Atmos. Sci.*, **48**, 1348–1359.

———, 1991b: The saturation of gravity waves in the middle atmosphere. Part II: Development of Doppler-spread theory, *J. Atmos. Sci.*, **48**, 1360–1379.

———, 1991c: The saturation of gravity waves in the middle atmosphere. Part III: Formation of the turbopause and of turbulent layers beneath it, *J. Atmos. Sci.*, **48**, 1380–1385.

———, 1993: The saturation of gravity waves in the middle atmosphere. Part IV: Cutoff of the incident wave spectrum, *J. Atmos. Sci.*, **50**, 3045–3060.

———, 1997a: Doppler-spread parameterization of gravity wave momentum deposition in the middle atmosphere. Part 1: Basic formulation, *J. Atmos. Solar Terr. Phys.*, **59**, 371–386.

———, 1997b: Doppler-spread parameterization of gravity wave momentum deposition in the middle atmosphere. Part 2: Broad and quasi monochromatic spectra, and implementation, *J. Atmos. Solar Terr. Phys.*, **59**, 387–400.

Lübken, F.-J., 1997: Seasonal variation of turbulent energy dissipation rates at high latitudes as determined by in situ measurements of neutral density fluctuations, *J. Geophys. Res.*, **102**, 13,441–13,456.

Manzini, E. and N.A. McFarlane, 1998: The effect of varying the source spectrum of a gravity wave parameterization in a middle atmosphere general circulation model, *J. Geophys. Res.*, **103**, 31,523–31,539.

McLandress, C., 1997: Sensitivity studies using the Hines and Fritts gravity wave drag parameterizations, in *Gravity Wave Processes: Their Parameterization in Global Climate Models*, 245–255, Springer-Verlag, Heidelberg.

Medvedev, A.S. and G.P. Klassen, 1995: Vertical evolution of gravity wave spectra and the parameterization of associated wave drag, *J. Geophys. Res.*, **100**, 25,841–25,853.

———, ———, and S.R. Beagley, 1998: On the role of an anisotropic gravity wave spectrum in maintaining the circulation of the middle atmosphere, *Geophys. Res. Lett.*, **25**, 509–512.

Scaife, A.A., N. Butchart, C.D. Warner, D. Stainforth, W. Norton, and J. Austin, 2000: Realistic Quasi-Biennial Oscillations in a simulation of the global climate, *Geophys. Res. Lett.*, **27**, 3481–3484.

Smith, S.A., D.C. Fritts, 1987: T.E. VanZandt, Evidence of a saturated spectrum of atmospheric gravity waves, *J. Atmos. Sci.*, **44**, 1404–1410.

Tsuda, T., T.E. VanZandt, M. Mizumoto, S. Kato, and S. Fukao, 1991: Spectral analysis of temperature and Brunt-Vaisala frequency fluctuations observed by radiosondes, *J. Geophys. Res.*, **96**, 17265–17278.

Warner, C.D. and M.E. McIntyre, 1996: On the propagation and dissipation of gravity wave spectra through a realistic middle atmosphere, *J. Atmos. Sci.*, **53**, 3213–3235.

Warner, C.D. and M.E. McIntyre, 1999: Toward an ultra-simple spectral gravity wave parameterization for general circulation models, *Earth Planet Space*, **51**, 475–484.

——— and ———, 2001: An ultra-simple spectral parameterization for non-orographic gravity waves, *J. Atmos. Sci.*, **58**, 1837–1857.